Integrated Plant and Control Design of a Continuously Variable Transmission

Integrated Plant and Control Design of a Continuously Variable Transmission

Chyannie A. Fahdzyana, Mauro Salazar, Theo Hofman

***Abstract*—This paper presents an optimization framework to design the components and the controller of a Continuously Variable Transmission (CVT) in an integrated manner. Specifically, we aim at reducing the mass of the transmission and the leakage losses that occur in the system. To do so, we first formulate the joint plant and control design problem including the corresponding objectives and constraints. Thereafter, we propose a proportional integral structure for the design of the CVT ratio control. The combined plant and control design problem is formulated as a nonlinear multi-objective optimization problem, and is simultaneously solved using an interior point optimization method. We evaluate the obtained design on the Worldwide Harmonized Light Vehicles Test Cycle (WLTC) as well as on more aggressive driving scenarios, and demonstrate that the optimized CVT design is always capable of realizing the required driving performance. Additionally, we study the impact of the plant design parameters on the control performance by analyzing the coupling strength between the subproblems. Thereby, the pulley radius is found to have the strongest influence in the resulting leakage losses that occur at the variator level. Finally, leveraging the presented design framework, we show that up to 13% and 18% reduction in the CVT variator mass and on leakage losses, respectively, can be achieved without compromising the desired ratio trajectory over a representative dynamic driving cycle.**

***Index Terms*—optimization, multi-objective optimization, continuously variable transmission, co-design, system design, simultaneous design**

I. Introduction

DUE TO stricter emission regulations as well as increasing demands on reducing the cost of ownership, reducing its energy consumption is becoming one of the most important design goals of a vehicle. In the past decade, as an effort to realize more energy-efficient vehicles with a lower cost-of-ownership, a considerable amount of research on optimal vehicle design strategies have been conducted, including the development of suitable controllers for energy management [1]–[7], or in combination with optimal powertrain component sizing [8]–[11]. In addition to the energy management, topology, and component sizes, the choice of the powertrain components (e.g., the type of e-machine, the transmission) has a significant influence on the total cost-of-ownership of the vehicle as well as its performance.

Unlike other types of transmission, a CVT allows the primary power source to be operated at the operating points that correspond to the highest energy efficiency regions [12], [13]. This advantage is attributed to the ability to continuously vary the speed ratio values, allowing the required speed and torque of the wheels to be matched with any speed and torque of the propulsion source (e.g., engine, electric machine). Furthermore, a CVT also offers a smooth torque shifting performance, which is beneficial in terms of comfort. A schematic diagram of a generic powertrain architecture equipped with a CVT is shown in Fig. 1.

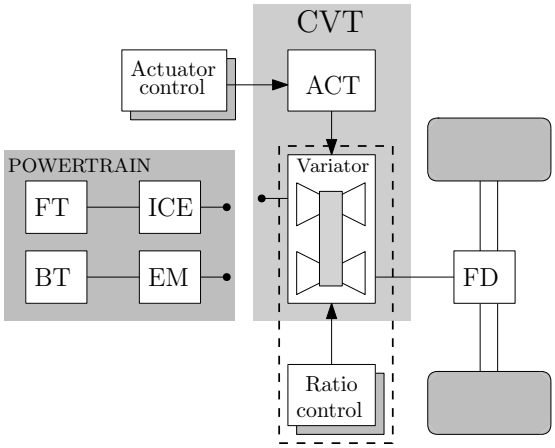

Fig. 1. Powertrain architecture equipped with a belt-driven CVT system, which consists of a variator and an actuation system (ACT). The powertrain type can be of a conventional type with internal combustion engine (ICE) and a fuel tank (FT), or, e.g., an all-electric type with an electric machine (EM) and battery (BT). The transmission is connected to the wheels via a final drive ratio (FD). The actuation and ratio control components are indicated by shaded blocks. The co-design problem discussed in this article is highlighted by the dashed line.

Arguably, a CVT offers several benefits for the performance of a vehicle. Yet, the energy efficiency of the system itself still has margins for improvement: Compared to other types of vehicle transmission, a belt-driven CVT has a relatively lower efficiency (84%), whereas a manual (MT) and automatic transmissions (AT) typically have a system efficiency of around 96% and 85%, respectively [14]. Besides, CVT requirements are also changing. Higher power density, lower transmission energy consumption, weight and, of course, cost are desired. This strengthens the motivation to redesign the current CVTs available on the market, maximizing their efficiency whilst minimizing their size, which calls for integrated plant and control optimal design methods, also known as *co-design*.

In this paper, we present a design optimization framework for CVT systems where the plant and control design are jointly optimized. The aim of the design is to achieve a lighter CVT system as well as improved energy consumption, without compromising the required driving performance for different scenarios (e.g., highway driving, harsh braking, and driving uphill).

A. Literature Review

Several theories and solution strategies related to the field of co-design have been proposed in the literature. Traditionally, combined plant and control optimization is conducted in a sequential (first plant, then control) or iterative manner (repeated sequential process) [15]. However, these strategies fail to account for the interdependency (coupling) between plant and control, yielding a suboptimal system design. Hence, in order to achieve an optimal system design, the coupling between the plant and its controller has to be considered during the design process, which can be done by several optimization methods, namely simultaneous/all-in one, nested/bi-level, and partitioned strategies [16]–[18].

In the past few years, co-design has been implemented for multiple applications, which includes turbine design [19], robotics [20], and in the automotive field [21]–[23]. The greater part of the existing research favored the use of the nested optimization framework [23]–[26], with Linear Quadratic Regulator (LQR) [27], Dynamic Programming (DP) [28], Convex Programming [25] as the solution formulation of the control subproblem. The popularity of this co-design strategy is attributed to the advantage of the formulation, which allows optimal control solution techniques to be directly applied to the control subproblem. Despite the benefit, the nested approach is restricted to the assumption that an optimal controller always exists for the system [18]. Additionally, the computational efficiency of this approach depends on the control optimization algorithm [29]. For instance, if the control subproblem can be written in an LQR formulation, the nested strategy can be efficiently used to solve the optimization problem. However, if the control subproblem utilizes DP and consists of multiple state variables, the nested approach can run into computational issues.

Several researchers have investigated the use of simultaneous optimization strategies for integrated plant and control system design [30], [31], using open loop control techniques, whereby the control optimization finds the optimal input trajectory with no assumption on the control structure (e.g., state feedback). While this technique is useful in the design stage to explore the limitations of the system, in reality the closed loop control strategy is often needed to account for disturbance rejection and stability [32].

In order to improve the CVT energy efficiency and performance, several advances have been proposed in the literature. These include physically redesigning the CVT, by developing on-demand actuation systems [33] and belt design [34], [35], as well as improving the control strategy, e.g., the variator slip control strategy [36]. However, to the best of the authors' knowledge, the existing strategies treated the system design problem as two separate sub-problems, disconnecting the plant and its controller. Hence, in this paper, we study the obtained CVT systems using the integrated plant and control (co-design) framework.

B. Problem Formulation

To arrive at an improved and commercially attractive transmission for vehicles, the following key performance indicators (KPIs) are defined, namely:

- **Efficiency**: The new CVT design should have a lower energy consumption compared to the currently existing design to improve the transmission efficiency.
- **Mass**: The new CVT design should have a lower mass compared to the commercially available transmissions as it benefits the powertrain system in terms of energy consumption.
- **Performance**: The new CVT design should not compromise the ability to accurately follow the desired speed ratio trajectory for driving.

In this context, we formulate a co-design framework for a CVT system, whereby the aim of the new design is to realize the KPIs. Furthermore, we investigate the obtained optimized system design under different driving profiles, namely the WLTC which is used as a standard to assess the emission generation and energy consumption of a vehicle, as well as predefined driving profiles that consist of more aggressive behaviors (e.g., tip-in, uphill driving, harsh braking, etc). Without loss of generality, we limit ourselves to the co-design of the CVT for a given primary power source (engine).

C. Statement of Contributions

A preliminary version of this paper was presented at the 2020 American Control Conference (ACC) [37], where we discussed the difference of the resulting CVT design obtained from using a simultaneous optimization approach and that of a sequential approach for the WLTC using a proportional feedback control scheme. In this extended version, we implement a proportional integral controller for the design of the CVT ratio tracking control subproblem in order to achieve a better performance. Furthermore, we demonstrate the coupling between the plant and control design in a both qualitative and quantitative manner. Additionally, we validate the performance of the optimized CVT design in more demanding driving scenarios. Using the proposed design method, new insights in the design process and potential improvements of the systems are investigated.

D. Organization

The remainder of this paper is structured as follows. The modeling of the CVT dynamics and characteristics is presented in Section II. Following that, the proposed plant and control design formulation is elaborated in Section III. Section IV discusses the results of the study. Finally, the conclusions of this study as well as the recommendations for future research are summarized in Section V.

II. CVT Principle Modeling

In this section, we introduce the principles of operation as well as the system dynamics model of a pushbelt CVT.

A. Kinematic and Geometric Formulations

Generally, a CVT consists of multiple subsystems and components (Cf. Fig. 1), namely: (1) a variator, which consists of two sets of conical pulley sheaves; (2) a V-belt used to

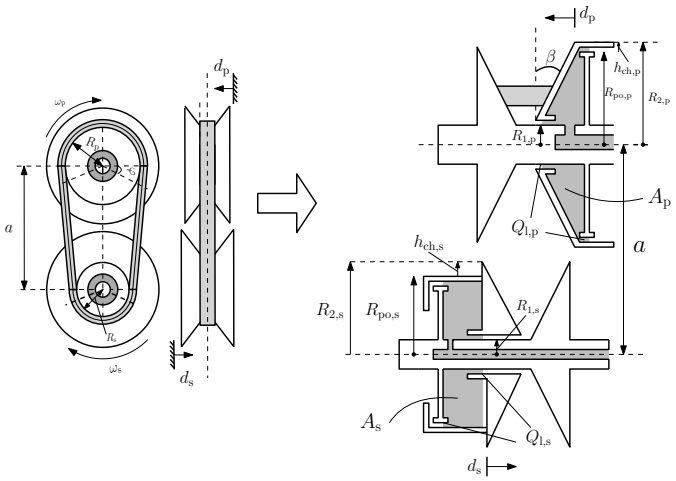

Fig. 2. CVT variator diagram.

transmit torque; (3) the actuation technology, which moves the pulley sheaves by realizing the required clamping force to perform shifting; and, finally, (4) the control system to ensure reliable operation. The CVT variator diagram is depicted in Fig. 2.

By horizontally moving the pulley sheaves on both the primary and secondary sides, the ratio of the input and output speed of a CVT is varied. The CVT geometric ratio is given by

$$r_\mathrm{g} = \frac{R_\mathrm{p}}{R_\mathrm{s}}\,, \tag{1}$$

where R_p and R_s are the primary and secondary running radii, which is the distance of the belt contact point from the center points of the corresponding pulleys, as shown in Fig. 2. Furthermore, due to the friction between the belt and the pulley, there exists a *slip* in the variator, which is the relative difference of the belt tangential speed of the primary and secondary pulley sets. The belt slip is given by

$$v = \frac{\omega_\mathrm{p} R_\mathrm{p} - \omega_\mathrm{s} R_\mathrm{s}}{\omega_\mathrm{p} R_\mathrm{p}}\,, \tag{2}$$

where ω_p and ω_s are the primary and secondary shaft rotational speed. For small slip values, the CVT ratio is defined as [33]

$$r_\mathrm{g} = \frac{R_\mathrm{p}}{R_\mathrm{s}} = \frac{\omega_\mathrm{s}}{\omega_\mathrm{p}}\,, \tag{3}$$

The positions of the movable pulley sheave yield different wrap angles $\varphi_\mathrm{p,s}$, defined as the span of the belt on the pulley sheaves, which are given by

$$\varphi_\mathrm{p} = \pi + 2\varphi\,,\ \varphi_\mathrm{s} = \pi - 2\varphi\,, \tag{4}$$

$$\varphi = \sin^{-1}\left(\frac{R_\mathrm{p} - R_\mathrm{s}}{a}\right)\,, \tag{5}$$

where a is the center distance between the primary and secondary pulleys, and φ_p and φ_s are the primary and secondary wrap angles, respectively. Mathematically, the relationship between the pulley horizontal position and running radius is given by

$$R_i = \frac{d_i}{2\tan(\beta)} + R_\mathrm{o}\,,\ \text{for } i = \{\mathrm{p},\mathrm{s}\}\,, \tag{6}$$

where β is the pulley wedge angle, d_p and d_s are the positions of the movable pulley sheaves. Furthermore, R_o is defined as the radius of the belt at $r_\mathrm{g} = 1$. By assuming that the span of the belt over the pulley is a perfect circle, the length of the belt can be expressed as

$$L_\mathrm{b} = 2\,a\,\cos(\varphi) + \varphi_\mathrm{p}\,R_\mathrm{p} + \varphi_\mathrm{s}\,R_\mathrm{s}\,, \tag{7}$$

which is a function of the center distance a and the primary and secondary wrap angles.

The movable pulley sheaves are enforced by the actuation of the CVT, which typically is a hydraulic system. The hydraulic actuation provides the required pressures that are applied to the movable pulley sheaves via oil inside the variator hydraulic cylinders, as shown in Fig. 2.

B. Variator Dynamics

Several transient models have been developed in order to capture the dynamical behavior of the CVT. Some are empirical models [38], [39], which are derived on the basis of measurements, and an analytical model in [40], which takes into account the pulley deformation that occurs during CVT operation. Because of the dependency on the availability of measurement data, the empirical models are not suitable to be used in the framework of co-design. Hence, we select the analytical model proposed by [40] to describe the behavior of the shifting dynamics

$$\dot{r}_\mathrm{g} = 2\,\omega_\mathrm{p}\,\Delta\,\frac{1+\cos^2(\beta)}{\sin(2\,\beta)}\,c(r_\mathrm{g})\,\left[\ln\frac{F_\mathrm{p}}{F_\mathrm{s}} - \ln\frac{F_\mathrm{p}}{F_\mathrm{s}}\Big|_\mathrm{ss}\right] \tag{8}$$

where ω_p is the primary rotational speed, Δ is the pulley deformation, $\frac{F_\mathrm{p}}{F_\mathrm{s}}$ is the clamping force ratio, and $\frac{F_\mathrm{p}}{F_\mathrm{s}}\big|_\mathrm{ss}$ is the steady-state clamping force ratio (at $\dot{r}_\mathrm{g} = 0$), which is the clamping force ratio needed to sustain a certain ratio value. The pulley deformation Δ in radians can be directly expressed as an empirical function of F_s [40],

$$\Delta = (1 + 0.02\,(F_\mathrm{s} - 20)) \cdot 10^{-3}\,. \tag{9}$$

The dynamics of $\dot{r}_\mathrm{g}$ depends on the balance between the applied and steady-state clamping force ratio, as well as the term $c(r_\mathrm{g})$, which is a nonlinear term that relates the dimensionless speed ratio and the logarithmic value of the steady-state clamping force ratio [40]. When the CVT is shifting ($\dot{r}_\mathrm{g} \neq 0$), $\left[\ln\frac{F_\mathrm{p}}{F_\mathrm{s}} - \ln\frac{F_\mathrm{p}}{F_\mathrm{s}}\big|_\mathrm{ss}\right] \neq 0$. Also, when the CVT ratio is held at a constant value ($\dot{r}_\mathrm{g} = 0$), $\left[\ln\frac{F_\mathrm{p}}{F_\mathrm{s}} - \ln\frac{F_\mathrm{p}}{F_\mathrm{s}}\big|_\mathrm{ss}\right] = 0$. The term $c(r_\mathrm{g})$ is expressed as a quadratic function of r_g [37],

$$c(r_\mathrm{g}) = c_1\,r_\mathrm{g}^2 + c_2\,r_\mathrm{g} + c_3\,, \tag{10}$$

where the fitted coefficients c_i are summarized in Table I. The steady-state clamping force ratio $\frac{F_\mathrm{p}}{F_\mathrm{s}}\big|_\mathrm{ss}$ necessary to sustain a certain constant r_g value, can be calculated analytically via the pressure distribution on the variator and belt, as can be found in [40]. Additionally, it is also observed that $\frac{F_\mathrm{p}}{F_\mathrm{s}}\big|_\mathrm{ss}$ depends on the wedge angle as well as on the load torque of the transmission. Hence, the steady-state clamping force ratio can

TABLE I
FITTED COEFFICIENTS a_{ij}, b_i, c_i

	value		value		value
a_{11}	11.9274	a_{12}	-5.6474	a_{13}	0.5647
a_{21}	-71.9417	a_{22}	31.3774	a_{23}	-2.9309
a_{31}	57.2683	a_{32}	-24.5247	a_{33}	3.2337
b_1	1.4741	b_2	0.4088	-	-
c_1	5.8553	c_2	2.8134	c_3	0.3832

be approximated as a function of ratio r_{g}, wedge angle β, and torque ratio $\Upsilon(.)$ [37]:

$$\left.\frac{F_{\mathrm{p}}}{F_{\mathrm{s}}}\right|_{\mathrm{ss}} = a_1(\beta) r_{\mathrm{g}}^2 + a_2(\beta) r_{\mathrm{g}} + a_3(\beta) + b_1 \Upsilon(\beta)^2 + b_2 \Upsilon(\beta)\,, \tag{11}$$

where the coefficients $a_{\mathrm{i}}(.)$ of the model in (11) are expressed as a function of the wedge angle β as

$$a_i(\beta) = a_{i1}\,\beta^2 + a_{i2}\,\beta + a_{i3}\,, \tag{12}$$

where $i = \{1, 2, 3\}$. The torque ratio $\Upsilon(.)$ here is defined as the ratio between the transmitted and maximum possible torque, [41]:

$$\Upsilon = \frac{T_{\mathrm{p}} \cos(\beta)}{2\,\overline{\mu}_{\mathrm{cvt}}\, R_{\mathrm{p}}\, F_{\mathrm{s}}}\,, \tag{13}$$

where T_{p} is the primary torque, F_{s} is the secondary clamping force, and $\overline{\mu}_{\mathrm{cvt}}$ is the maximum traction coefficient of the CVT. The found fit coefficients are listed in Table I.

III. INTEGRATED SYSTEM DESIGN FORMULATION

In this section, we formulate the simultaneous integrated plant and control system design method for the case study of CVT based on the desired key performance indicators (KPIs). First, we start with the discussion of the plant design problem, which is related to the physical characteristics of the CVT variator system. Second, we derive the control design formulation that is related to the system efficiency and performance. Finally, we elaborate the proposed controller structure considered in this study.

A. Plant Design Problem

Below, we discuss the plant design problem related to the variator design.

1) Minimizing variator mass: A scalable variator model that approximates the mass of the variator has been derived in [37],

$$M_{\mathrm{v}} = \rho_{\mathrm{pu}} V_{\mathrm{pu}} + \rho_{\mathrm{b}} V_{\mathrm{be}}\,, \tag{14}$$

with

$$V_{\mathrm{pu}} = \frac{2\pi}{3} \sum_{i=\{p,s\}} (R_{2,i} - R_{1,i}) \tan(\beta)(R_{2,i}^2 + R_{1,i}^2 + R_{1,i} R_{2,i}) \tag{15}$$

and

$$V_{\mathrm{be}} = \frac{b_1 + b_2}{2}\, b_3\, L_{\mathrm{b}}\,, \tag{16}$$

where L_{b} is the length of the belt, b_1 and b_2 are the belt element's widths, and b_3 is the belt element height. Additionally, the CVT pulley dimensions determine transmission ratio coverage, as the maximum and minimum speed ratio values are determined by the design of the pulley sheaves, such that

$$\overline{r}_{\mathrm{g}} = \frac{R_{2,\mathrm{p}} - \delta_{\mathrm{o}}}{R_{1,\mathrm{s}} + \delta_{\mathrm{i}}}\,,\; \underline{r}_{\mathrm{g}} = \frac{R_{1,\mathrm{p}} + \delta_{\mathrm{i}}}{R_{2,\mathrm{s}} - \delta_{\mathrm{o}}}\,, \tag{17}$$

where δ_{o} and δ_{i} are the belt margin from the pulley edges. The CVT center distance a is directly determined by the pulley outer radii R_2 as

$$a = R_{2,\mathrm{p}} + R_{2,\mathrm{s}} + \delta_{\mathrm{a}}\,, \tag{18}$$

where δ_{a} is the minimum distance between the two pulleys. Here, we consider that $R_{1,\mathrm{p}} = R_{1,\mathrm{s}} = R_1$, and $R_{2,\mathrm{p}} = R_{2,\mathrm{s}} = R_2$. Therefore, the plant design objective is to minimize the dimensionless variator mass as

$$\min_{\mathbf{x}_{\mathrm{P}}} J_{\mathrm{P}} = \min_{\mathbf{x}_{\mathrm{P}}} \frac{M_{\mathrm{v}}(\mathbf{x}_{\mathrm{P}})}{M_{\mathrm{v,o}}}\,, \tag{19}$$

whereby the variator mass is defined as a function of the plant design variables $M_{\mathrm{v}}(\mathbf{x}_{\mathrm{P}})$, normalized by the nominal variator mass $M_{\mathrm{v,o}}$, obtained from the baseline parameters. Further, we select the plant design parameters to be the pulley wedge angle, shaft radius, and pulley outer radius, $\mathbf{x}_{\mathrm{P}} = [\beta, R_1, R_2]$. The minimization problem in (19) is to be solved subject to a set of plant design constraints, $g_{\mathrm{P},i}$:

$$g_{\mathrm{P},1} : \beta \in [\underline{\beta}, \overline{\beta}]\,, \tag{20a}$$

$$g_{\mathrm{P},2} : R_1 \in [\underline{R}_1, \overline{R}_1]\,, \tag{20b}$$

$$g_{\mathrm{P},3} : R_2 \in [\underline{R}_2, \overline{R}_2]\,, \tag{20c}$$

whereby the minimum value of the wedge angle $\underline{\beta}$ is determined by the maximum friction coefficient between the belt and the pulley sheave $\overline{\mu}$ [42], [35], yielding

$$\tan(\underline{\beta}) - \overline{\mu} > 0\,. \tag{20d}$$

For instance, here we utilize $\overline{\mu} = 0.1228$, resulting in $\underline{\beta} = 7^o$. Additionally, following that $R_{1,\mathrm{p}} = R_{1,\mathrm{s}}$ and $R_{2,\mathrm{p}} = R_{2,\mathrm{p}}$, we have $\underline{r}_{\mathrm{g}} = 1/\overline{r}_{\mathrm{g}}$. Rearranging (17), we arrive at a constraint that relates R_1 and R_2 as

$$g_{\mathrm{P},7} : R_2\, \underline{r}_{\mathrm{g}} - R_1 - \underline{r}_{\mathrm{g}}\, \delta_{\mathrm{o}} - \delta_{\mathrm{i}} = 0\,, \tag{20e}$$

where $\underline{r}_{\mathrm{g}}$ and $\overline{r}_{\mathrm{g}}$ are determined based on the towing characteristics and the required vehicle maximum speed, respectively. In this work, the values of $\underline{r}_{\mathrm{g}}$ and $\overline{r}_{\mathrm{g}}$ are given.

The lower boundary value for the inner pulley radius $\underline{R}_1$ is determined by the diameter of the shaft $d = 2\,\underline{R}_1$,

$$g_{\mathrm{P},8} : \frac{16\,(\overline{T}_{\mathrm{p}})}{\pi\,(2\,\underline{R}_1)^3} - \overline{\tau} \leq 0\,, \tag{20f}$$

which is a function of the maximum allowable shear stress $\overline{\tau}$ and the maximum propulsive torque $\overline{T}_{\mathrm{p}}$ at the primary shaft.

B. Control Design Problem

In this section the control design problem related to the improvement of the transmission efficiency, while still satisfying the required system performance, will be analyzed in more detail:

1) Minimizing the leakage losses: The power consumption of a CVT is mainly determined by the variator and the actuation system. In this paper we assume that the slip that occurs in the system is very small, hence negligible. The minimum required actuation power to move the pulley sheaves at the variator level P_{v} is given by

$$P_{\mathrm{v}} = \sum_{i \in \{\mathrm{p,s}\}} F_i \, v_i \,, \tag{21}$$

where F_i is the clamping force and v_i is the pulley sheave horizontal speed. There is also an additional power loss in the variator due to leakage in the hydraulic pulley cylinders in the variator (Fig. 2). This loss is proportional to the applied pressure, formulated as

$$P_{\mathrm{l}} = \sum_{i \in \{\mathrm{p,s}\}} Q_{\mathrm{l},i} \, p_i \,, \tag{22}$$

where $Q_{\mathrm{l},i}$ is the leakage flow, and p_i is the applied clamping pressure. The leakage flow is given by

$$Q_{\mathrm{l},i} = C_{\mathrm{l},i} \, p_i \,, \tag{23}$$

where $C_{\mathrm{l},i}$ is the leakage coefficient. Finally, the clamping pressure p_{i} is expressed as a function of the required clamping force to actuate the pulley sheaves F_{i}:

$$p_i = \frac{F_i - F_{\mathrm{cf},i}}{A_i} \,, \tag{24}$$

where $F_{\mathrm{cf},i}$ is the centrifugal force due to the oil rotation inside the pulley cylinder, and A_i is the cylinder surface area:

$$A_i = \pi (r_{\mathrm{po},i}^2 - r_{\mathrm{pi},i}^2) \,, \tag{25}$$

where $r_{\mathrm{po},i}$ and $r_{\mathrm{pi},i}$ are the outer and inner radius of the oil chamber, respectively. The surface areas of the primary and secondary pulley cylinders are determined based on the required pulley thrust ratio [42], such that

$$\frac{A_{\mathrm{p}}}{A_{\mathrm{s}}} \geq \max \left(\frac{F_{\mathrm{p}}}{F_{\mathrm{s}}} \right) \,, \tag{26}$$

which yields $A_{\mathrm{p}} \geq A_{\mathrm{s}}$. Furthermore, the piston radii $r_{\mathrm{po},i}$, $r_{\mathrm{pi},i}$ (see Fig. 2) depend on the size of the variator pulleys as

$$r_{\mathrm{po},i} = R_2 - h_{\mathrm{ch},i} \,, \tag{27}$$

with $h_{\mathrm{ch},i}$ as a constant representing the distance between the pulley outer radius and the hydraulic cylinder piston radius. Following (26), due to the relation $A_{\mathrm{p}} \geq A_{\mathrm{s}}$, the secondary piston radius is smaller than the primary one. Therefore, the piston radii can be formulated as

$$\begin{aligned} r_{\mathrm{po},p} &= R_2 - h_{\mathrm{ch,p}} \,, \\ r_{\mathrm{po},s} &= \frac{r_{\mathrm{po},p}}{f_{\mathrm{p}}} \,, \end{aligned}$$

where f_{p} is a constant. Moreover, the centrifugal force $F_{\mathrm{cf},i}$ in the cylinders that occurs during operation is influenced by the pulley dimensions as well as the rotational speed ω_i. The expression of this force component is found in [43] to be

$$F_{\mathrm{cf},i} = \frac{\pi}{4} \, \rho_{\mathrm{o}} \, (r_{\mathrm{po},i}^4 - r_{\mathrm{in},i}^4) \, \omega_i^2 \,. \tag{28}$$

The control optimization objective $J_{\mathrm{C}}(.)$ related to the CVT efficiency is defined as the minimization of the power loss due to leakage in the pulley hydraulic cylinders as a function of both the plant and control design variables $\mathbf{x}_{\mathrm{P}}$ and $\mathbf{x}_{\mathrm{C}}$, respectively, as

$$\min_{\mathbf{x_C}} J_{\mathrm{C}} = \min_{\mathbf{x}_{\mathrm{C}}} \frac{1}{E_{\mathrm{l,o}}} \int_0^{t_{\mathrm{f}}} P_{\mathrm{l}}(\mathbf{x}_{\mathrm{P}}, \mathbf{x}_{\mathrm{C}}, t) \, \mathrm{d}t \,, \tag{29}$$

from initial time $t = 0$ to final time $t = t_{\mathrm{f}}$ where we normalize the energy leakage flow losses with the nominal energy leakage flow losses $E_{\mathrm{l,o}}$, subject to a set of design constraints which will be explained further below in this section. Here, the normalization value $E_{\mathrm{l,o}}$ is selected to be the leakage losses of the baseline design. The control design variable $\mathbf{x}_{\mathrm{C}}$ influencing both the leakage losses and tracking performance will be introduced in the subsequent section.

2) Ratio tracking performance: One of the desired CVT performance criteria is the ability to accurately track the desired transmission ratio values that may yield the lowest energy usage of the powertrain over a driving cycle (e.g., WLTC); and/or, the required severe dynamic speed ratio (up- and downshift) changes during certain driving maneuvers. Hence, in this work, we enforce the performance of the CVT criterion as constraints on the maximum and minimum allowable ratio tracking error,

$$\underline{e} \leq e(t) \leq \overline{e} \,,$$

where e is the difference between the desired and actual speed ratio values.

3) Feedback Linearization Control Strategy: Several CVT ratio-control strategies have been considered in the existing literature, ranging from classical feedback control [33], through a combination of feedforward and feedback control [42], to fuzzy logic [44], [45]. In this work, we propose a closed-loop ratio-control strategy for the co-design of a CVT based on feedback linearization.

For a nonlinear system with state variable ξ, input u and output y that satisfies

$$\dot{\xi}(t) = f(\xi(t)) + g(\xi(t)) \, u(t) \,, \tag{30a}$$

$$y(t) = h(\xi(t)) \,, \tag{30b}$$

there exists a feedback-control input

$$u(t) = A(\xi(t)) + B(\xi(t)) \, v(t) \tag{30c}$$

that transforms the nonlinear system into an equivalent linear system [46].

Consider the dynamic shifting model in (8). By selecting the term $\left[\ln \frac{F_{\mathrm{p}}}{F_{\mathrm{s}}} - \ln \frac{F_{\mathrm{p,ss}}}{F_{\mathrm{s,ss}}} \right]$ as the system input $u(t)$, and $r_{\mathrm{g}}(t)$ as the state variable $\xi(t)$, the dynamic shifting model can be represented as the form

$$\dot{\xi}(t) = f(\xi(t), \mathbf{x}_{\mathrm{P}}) + g(\xi(t), \mathbf{x}_{\mathrm{P}}) \, u(t) \,, \tag{31}$$

$$\dot{r}_g(t) = \underbrace{\Theta(r_{\mathrm{g}}(t), \beta, \omega_{\mathrm{p}(t),t})}_{g(\xi(t), \mathbf{x}_{\mathrm{P}})} \, u(t) \,. \tag{32}$$

where $f(\xi(t), \mathbf{x}_{\mathrm{P}}) = 0$, and

$$\Theta(r_{\mathrm{g}}, \omega_{\mathrm{p}}, t) = 2 \, \omega_{\mathrm{p}}(t) \, \Delta \, \frac{1 + \cos^2 \beta}{\sin 2\beta} \, c(r_{\mathrm{g}}(t)) \,, \tag{33}$$

with the term $c(.)$ given in (10). In this work, the trajectory of $\omega_{\mathrm{p}}(t)$ is given. For $\omega_{\mathrm{p}}(t) \neq 0$, the term $\Theta(.)$ is nonzero. Thus, we can rewrite (8) to be

$$\dot{r}_{\mathrm{g}} = v(t)\,, \tag{34}$$

where $v(t)$ is the external control input. The system input $u(t)$ is then obtained as

$$u(t) = \begin{cases} \frac{v(t)}{2\,\omega_{\mathrm{p}}(t)\,\Delta\,\frac{1+\cos^2\beta}{\sin 2\beta}\,c(r_{\mathrm{g}}(t))} & \text{for } \omega_p(t) \neq 0\,, \\ 0 & \text{for } \omega_p(t) = 0\,. \end{cases} \tag{35}$$

Furthermore, we have the freedom to select the external control input v. An earlier study conducted in [37] has investigated the use of a proportional feedback controller for CVT design over the WLTC profile. To further improve the performance of the design, we employ a proportional integral controller to determine $v(t)$ as

$$v(t) = -K_{\mathrm{p}}\,e(t) - K_{\mathrm{i}} \int e(t)\,\mathrm{d}t\,, \tag{36}$$

where K_{p} and K_{i} are the controller gains, and $e(t) = r_{\mathrm{g}}(t) - r_{\mathrm{g,r}}(t)$ is the difference between the desired and actual ratio trajectory. The primary clamping force $F_{\mathrm{p}}(t)$ can be reconstructed from the input signal $u(t)$ as

$$F_{\mathrm{p}}(t) = \exp\left[u(t) + \ln\left(\left.\frac{F_{\mathrm{p}}}{F_{\mathrm{s}}}\right|_{\mathrm{ss}}(t)\right)\right] F_{\mathrm{s}}(t)\,, \tag{37}$$

where $u(t)$ is expressed in (35), and $\left.\frac{F_{\mathrm{p}}}{F_{\mathrm{s}}}\right|_{\mathrm{ss}}$ is given in (11). The secondary clamping force $F_{\mathrm{s}}(t)$ is known over the trajectory, and is given by [41] as

$$F_{\mathrm{s}}(t) = \frac{\cos(\beta)\,(|T_{\mathrm{p}}(t)| + S_{\mathrm{f}}\,T_{\max})}{2\,\overline{\mu}_{\mathrm{cvt}}\,R_{\mathrm{p}}}\,, \tag{38}$$

where S_{f} is a safety factor for the clamping force to prevent excessive slip, T_{p} is the primary torque, $T_{\max}$ is the maximum torque that can be delivered by the engine, $\overline{\mu}_{\mathrm{cvt}}$ is the effective traction coefficient, and R_{p} is the primary running radius.

The minimization problem proposed in (29) is subject to a set of equality control design constraints,

$$h_{\mathrm{C},1} : e(t) = r_{\mathrm{g}}(t) - r_{\mathrm{g,r}}(t)\,, \tag{39a}$$

$$h_{\mathrm{C},2} : E(t) = \int e(t)\,\mathrm{d}t\,, \tag{39b}$$

$$h_{\mathrm{C},3} : \dot{e}(t) = \dot{r}_{\mathrm{g}}(t) - \dot{r}_{\mathrm{g,r}}(t)\,, \tag{39c}$$

$$= \underbrace{-K_{\mathrm{p}}\,e(t) - K_{\mathrm{i}}\,E(t)}_{v(t)} - \dot{r}_{\mathrm{g,r}}(t)\ \ , \tag{39d}$$

$$h_{\mathrm{C},4} : e(0) = 0\,, \tag{39e}$$

and inequality control design constraints that bound the acceptable tracking error:

$$g_{\mathrm{C},1} : \underline{e} - e(t) \leq 0\,, \tag{39f}$$

$$g_{\mathrm{C},2} : e(t) - \overline{e} \leq 0\,, \tag{39g}$$

$$g_{\mathrm{C},3} : \underline{E} - E(t) \leq 0\,, \tag{39h}$$

$$g_{\mathrm{C},4} : E(t) - \overline{E} \leq 0\,, \tag{39i}$$

$$g_{\mathrm{C},5} : \underline{\dot{e}} - \dot{e}(t) \leq 0\,, \tag{39j}$$

$$g_{\mathrm{C},6} : \dot{e}(t) - \overline{\dot{e}} \leq 0\,. \tag{39k}$$

C. Simultaneous design problem and implementation

The combined optimization problem can be formulated as the weighted sum of the plant, P, and control, C, design objectives, denoted as $w_i \cdot J_{\mathrm{i}}$ for $i \in \{\mathrm{P}, \mathrm{C}\}$ as follows:

$$\min_{\mathbf{x}_{\mathrm{P}} \subseteq \mathfrak{X}_{\mathrm{P}}, \mathbf{x}_{\mathrm{C}} \subseteq \mathfrak{X}_{\mathrm{C}}} w_{\mathrm{P}}\,J_{\mathrm{P}}(\mathbf{x}_{\mathrm{P}}) + w_{\mathrm{C}}\,J_{\mathrm{C}}(\mathbf{x}_{\mathrm{P}}, \mathbf{x}_{\mathrm{C}})\,, \tag{40}$$

where $w_{\mathrm{P}} + w_{\mathrm{C}} = 1$, $w_{\mathrm{P}}, w_{\mathrm{C}} \in [0, 1]$. The feasible plant design set $\mathfrak{X}_{\mathrm{P}}$ is then given by

$$\mathfrak{X}_{\mathrm{P}} = \left\{\ \mathbf{x}_{\mathrm{P}} = [\beta, R_1, R_2] : (20)\ \right\}. \tag{41}$$

Similarly, we define the feasible control design set $\mathfrak{X}_{\mathrm{C}}$ as

$$\mathfrak{X}_{\mathrm{C}} = \left\{\ \mathbf{x}_{\mathrm{C}} = [K_{\mathrm{p}}, K_{\mathrm{i}}] : (39)\ \right\}. \tag{42}$$

Furthermore, in (40), it is demonstrated that the plant design parameters $\mathbf{x}_{\mathrm{P}}$ influence the control objective function J_{C}, indicating the coupling between the plant and its control. The integrated plant and control design problem is accordingly formulated as a static optimization problem, whereby the time-dependent system dynamics is discretized using the trapezoidal method, which takes the general form

$$x_{k+1} = x_k + \frac{\Delta t}{2}(f(x_k, u_k) + f(x_{k+1}, u_{k+1}))\,, \tag{43}$$

where Δt is the discretization step, and $k \in \{0, 1, ..., N\}$, with the total number of discretized points $N = \frac{t_{\mathrm{f}} - t_0}{\Delta t}$.

IV. Results and Discussion

In this section, the results of the proposed co-design problem are discussed. The proposed optimization framework is parsed with YALMIP [47] and solved using the IPOPT solver [48] provided by the OPTI toolbox for the MATLAB interface [49]. The computational time that it takes to optimize the CVT design over the WLTC for one set of optimization weights $w_{\mathrm{P}}, w_{\mathrm{C}}$ is approximately 1000 s, which is performed on a computer with Intel Core i7-7700HQ CPU 2.8 GHz processor with 32 GB RAM. Here, we evaluate the design over two different driving profiles: (i) a WLTC drive cycle, and (ii) other (more aggressive) driving scenarios that are, typically, not covered in WLTC. These additional driving maneuvers are

1) *Tip-in*: When the driver presses the accelerator pedal, the engine speed and torque rapidly increase within a short amount of time.
2) *Harsh braking*: During this maneuver, the vehicle speed reduces rapidly. However, the engine torque stays constant.
3) *Hill-drive*: When the driver is going uphill. The ratio of the CVT stays at a low value.
4) *Pressure gradient*: The engine and vehicle speed are kept constant, while the engine torque is increased.
5) *Manual upshift high rpm*: Ratio shift from low to high ratio for high engine speed.
6) *Manual downshift high rpm*: Ratio shift from high to low ratio for high engine speed.

Further, the obtained new CVT variator design will be compared to a baseline design, which is one of the commercially available CVT types for passenger cars.

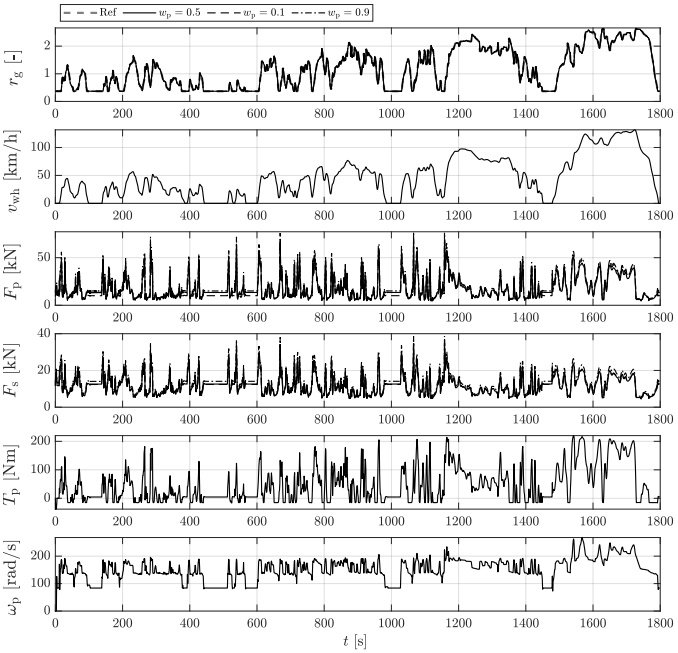

Fig. 3. Performance results of the optimized CVT design on the WLTC for different weight combinations.

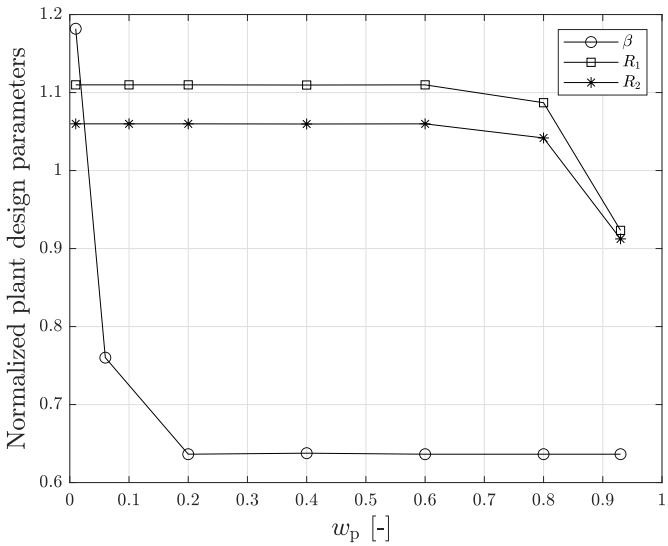

Fig. 4. Plot of the normalized plant design parameters as function of weight factor w_P. Normalization values: $\beta_\mathrm{o} = 11^o$, $R_{1,\mathrm{o}} = 23.5\,\mathrm{mm}$, $R_{2,\mathrm{o}} = 83.5\,\mathrm{mm}$.

A. Trade-off Between Plant and Control Design on the WLTC

In this subsection, we show the relationship between the plant and control design optimization over the WLTP drive cycle. To highlight the trade-off between the plant and control design, we investigate the results of the proposed design optimization obtained with different values of optimization weight w_P, which are summarized in Table II. The resulting performance of the optimized CVT with $w_\mathrm{P} = \{0.1\,,\,0.5\,,\,0.9\}$ is depicted in Fig. 3.

It is observed that compared to the baseline design, for $w_\mathrm{P} = w_\mathrm{C}$, the plant design can be significantly reduced by $\Delta J_\mathrm{P} = -13\%$ and the leakage losses by $\Delta J_\mathrm{C} = -18\%$.

For the case of $w_\mathrm{P} > w_\mathrm{C}$, the optimized variator mass is found to be the lowest out of the given cases $M_\mathrm{v} = 5.1$ kg, and the corresponding leakage losses the highest $E_\mathrm{l} = 29.8$ kJ, respectively. Conversely, for $w_\mathrm{P} < w_\mathrm{C}$, the obtained result yields the largest plant design cost $M_\mathrm{v} = 8.2$ kg, yet the control cost is found to be the lowest $J_\mathrm{C} = 13.9$ kJ. Furthermore, we evaluate the performance (tracking error) of the optimized CVT design over the WLTC. As shown in Fig. 3, it is found that all the optimized designs obtained with $w_\mathrm{P} \in \{0.1\,,\,0.5\,,\,0.9\}$ are able to track the reference ratio trajectory within the desired accuracy as set by the defined constraints. Although all the different designs are capable of satisfying the required performance, the clamping forces for that of the optimized CVT with $w_\mathrm{P} = 0.9$ are higher in comparison to the results obtained with other optimization weight values. This is attributed to the fact that as the weight factor increases, the less emphasis is put on minimizing the control design problem (leakage losses), which is directly determined by the clamping pressures. The resulting plant design parameters $\mathbf{x}_\mathrm{P}$ for different optimization weights are depicted in Fig. 4.

B. Coupling Strength Between Plant and Control Problem

Here, we further analyze the relationship between the plant and control design problem in a quantitative manner based on the Karush-Kuhn-Tucker (KKT) conditions for (local) optimality. The obtained plant design parameters $\mathbf{x}_\mathrm{P}$ represent the system optimal design solution if they minimize the combined plant and control optimization objective J. Given a general multi-objective optimization problem

$$\min_{\mathbf{x}_\mathrm{P},\mathbf{x}_\mathrm{C}} w_\mathrm{P} J_\mathrm{P}(\mathbf{x}_\mathrm{P}) + w_\mathrm{C} J_\mathrm{C}(\mathbf{x}_\mathrm{P},\mathbf{x}_\mathrm{C})\,, \tag{44}$$

subject to a set of equality and inequality constraints

$$\mathbf{h}(\mathbf{x}_\mathrm{P},\mathbf{x}_\mathrm{C}) = 0\,, \mathbf{g}(\mathbf{x}_\mathrm{P},\mathbf{x}_\mathrm{C}) \leq 0\,, \tag{45}$$

using the KKT first order necessary conditions for optimality for the combined plant and control optimization formulation, the set $\mathbf{x}_\mathrm{P}^\star$ are the (local) optima, given that

$$\begin{aligned}&\frac{\partial J_\mathrm{P}(\mathbf{x}_\mathrm{P}^\star)}{\partial \mathbf{x}_\mathrm{P}} + \lambda^\top \frac{\partial \mathbf{h}(\mathbf{x}_\mathrm{P}^\star,\mathbf{x}_\mathrm{C})}{\partial \mathbf{x}_\mathrm{P}} + \nu^\top \frac{\partial \mathbf{g}(\mathbf{x}_\mathrm{P}^\star,\mathbf{x}_\mathrm{C})}{\partial \mathbf{x}_\mathrm{P}} \\ &+ \frac{w_\mathrm{C}}{w_\mathrm{P}} \frac{\partial J_\mathrm{C}^\star(\mathbf{x}_\mathrm{P}^\star,\mathbf{x}_\mathrm{C})}{\partial \mathbf{x}_\mathrm{P}} = 0\,,\end{aligned} \tag{46}$$

and

$$\mathbf{h}(\mathbf{x}_\mathrm{P}^\star,\mathbf{x}_\mathrm{C}^\star) = 0\,, \mathbf{g}(\mathbf{x}_\mathrm{P}^\star,\mathbf{x}_\mathrm{C}^\star) \leq 0\,, \tag{47}$$

where λ and ν are the Lagrange multipliers. The coupling strength between plant and control design problem can be quantified by using the KKT first order optimality criterion for combined plant and control optimization problem [16] as

$$\Gamma = \frac{w_\mathrm{C}}{w_\mathrm{P}} \frac{\partial J_\mathrm{C}(\mathbf{x}_\mathrm{P},\mathbf{x}_\mathrm{C})}{\partial \mathbf{x}_\mathrm{P}}\bigg|_{\mathbf{x}_\mathrm{P}^\star,\mathbf{x}_\mathrm{C}^\star}\,, \tag{48}$$

where Γ is evaluated at the optimal J_C, $\mathbf{x}_\mathrm{P}$, and $\mathbf{x}_\mathrm{C}$. It can be seen that Γ appears in (46) as a term that describes the dependency of the control objective on the plant design parameters. If there is no influence from the plant design parameter on the control design formulation, the coupling term

TABLE II
OPTIMIZATION RESULTS: WLTC

Parameters	Description	Baseline	$w_{\mathrm{P}} = w_{\mathrm{C}}$	$w_{\mathrm{P}} < w_{\mathrm{C}}$	$w_{\mathrm{P}} > w_{\mathrm{C}}$	Unit
w_{P}	Plant objective weight	0	0.5	0.1	0.9	–
w_{C}	Control objective weight	1	0.5	0.9	0.1	–
J_{P}	Plant objective	1	0.87	1.16	0.72	–
J_{c}	Control objective	1	0.84	0.59	1.7	–
M_{v}	Variator mass	7.1	6.2	8.2	5.1	kg
E_l	Leakage loss	17.57	14.4	13.9	29.8	kJ
β	Wedge angle	11.0	7.0	13.0	7.0	^{o}
$R_{1,\mathrm{p}}$	Primary pulley inner radius	23.5	26.1	26.1	22.9	mm
$R_{2,p}$	Primary pulley outer radius	85.5	88.5	88.5	79.5	mm
$R_{1,\mathrm{s}}$	Secondary pulley inner radius	24.0	27.1	26.1	22.9	mm
$R_{2,s}$	Secondary pulley outer radius	86.5	88.5	88.5	79.5	mm
a	Center distance	173.0	180.0	180.0	162.0	mm
K_{p}	Proportional gain	188.7	214.6	9.07	218	$1/s$
K_{i}	Integral gain	0.33	0.4	0.05	0.46	$1/\mathrm{s}^2$
T_{sim}	Computation time	455.8	1000	869.8	1074	s

Γ will be zero. A further point to be considered is that if the value of Γ is higher, then the impact (specified as the coupling strength) is higher, too. Using this formulation, the coupling strength between the plant and control problem in this work will be evaluated. The coupling strength vector for our problem is given by

$$\Gamma = \left[\frac{\partial J_{\mathrm{C}}(\mathbf{x}_{\mathrm{P}}, \mathbf{x}_{\mathrm{C}})}{\partial \beta} \quad \frac{\partial J_{\mathrm{C}}(\mathbf{x}_{\mathrm{P}}, \mathbf{x}_{\mathrm{C}})}{\partial R_1} \quad \frac{\partial J_{\mathrm{C}}(\mathbf{x}_{\mathrm{P}}, \mathbf{x}_{\mathrm{C}})}{\partial R_2} \right] \Bigg|_{\mathbf{x}_{\mathrm{P}}^\star, \mathbf{x}_{\mathrm{C}}^\star}, \tag{49}$$

which corresponds to $\Gamma = [3.99\,,\, 14.59\,,\, -90.82]$ when computed for $w_{\mathrm{P}} = w_{\mathrm{C}} = 0.5$. The nonzero value of Γ implies that changing the plant design parameters will have an effect on the control performance.

We explain the physical interpretation that can be inferred based on the coupling strength study. As indicated by the coupling strength values, it is disclosed that the influence of each plant design parameters on the control performance is different. Specifically, the plant design parameter with the strongest influence on the control objective (leakage losses) is the pulley radius R_2. This can be explained by the fact that the pulley sheave radius mainly determines the surface area of the hydraulic pulley piston in the variator. The shaft radius R_1 also plays a role in determining the control performance, albeit not as much as R_2. Additionally, the wedge angle β has the lowest impact on the control objective of the proposed design problem. This is because there is no direct dependency between the leakage losses and the value of β. However, the wedge angle does influence the ratio dynamics $\dot{r}_{\mathrm{g}}$ which, in turn, determines the required clamping force that realizes the desired CVT ratio trajectory.

C. Validation of the Design Model

In order to validate our optimized co-design results, we evaluate the optimized plant and control design parameters obtained for the WLTC profile (see Table II) on the predefined more aggressive driving scenarios. These alternative driving maneuvers are necessary conditions that must be realized by the CVT system. To demonstrate this design validation, we select the design obtained with $w_{\mathrm{P}} = 0.5$ that yields both lower plant and control objectives when compared to those of the baseline ($J_{\mathrm{P}} \leq 1$, $J_{\mathrm{C}} \leq 1$).

The performance of the optimized CVT design in the more aggressive driving scenarios is depicted in Fig. 5 to Fig. 10. It can be seen from these results that with the WLTC-optimized CVT plant and control design parameters, the system is very much capable of realizing the required performances for these alternative driving scenarios with sufficient accuracy.

Furthermore, we compare the resulting leakage losses of the optimized system design for all the considered driving scenarios. In order to do this, we introduce several notations corresponding to the different case studies to be evaluated, namely:

1) **Case 1**. Given the fixed baseline plant design parameters, we optimize the controller such that the leakage losses are minimized for each individual driving scenario (WLTC, tip-in, harsh braking, etc.).
2) **Case 2**. Using the optimized plant and control design parameters obtained from co-design on the WLTC on the additional driving scenarios (tip-in, harsh braking, etc.).
3) **Case 3**. Using the optimized plant and control design parameters obtained from co-design on each of the driving scenarios (WLTC, tip-in, harsh braking, etc.).
4) **Case 4**. Using the optimized plant design parameters obtained from co-design on the WLTC and additionally optimizing the controller such that the leakage losses are minimized to each of the driving scenarios other than the WLTC (tip-in, harsh braking, etc.).

First, we investigate Case 1, Case 2, and Case 3. The comparison of the leakage losses is shown in Fig. 11. We concluded that the WLTC-optimized plant and control design (Case 2) yields lower average leakage loss than that of the baseline during the WLTC scenario, but not for some of the other driving maneuvers. This is a consequence of both the optimized plant and control design parameters. The obtained pulley wedge angle β of Case 2 is lower than that of the baseline (7^o and 11^o, respectively), and due to the relation in (38), lower values of β yield higher required F_{s}. As the leakage losses are expressed as a function of the clamping pressures, higher clamping pressures result in increased leakage losses. Furthermore, the results of Case 3 show that when both the plant and control design are optimized for each individual

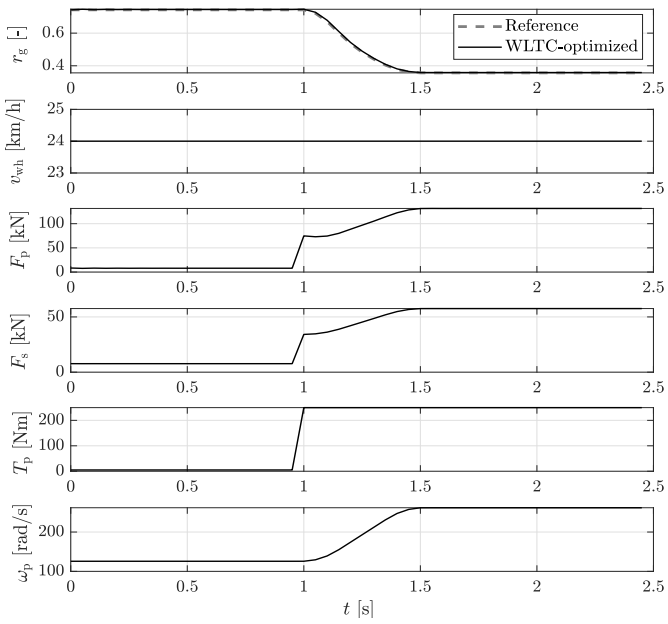

Fig. 5. Tip-in scenario.

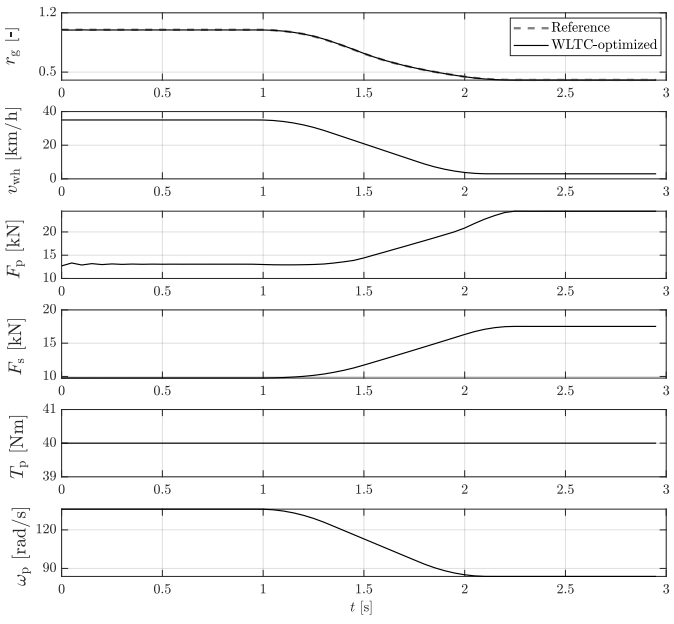

Fig. 6. Harsh braking scenario.

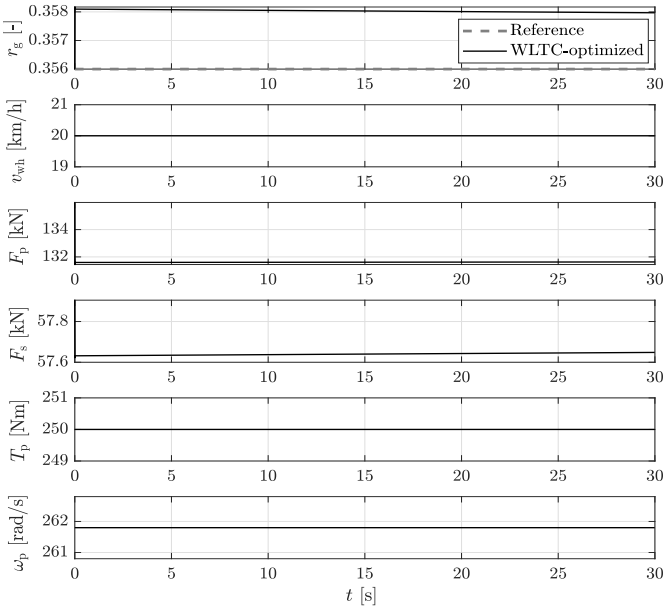

Fig. 7. Uphill driving scenario.

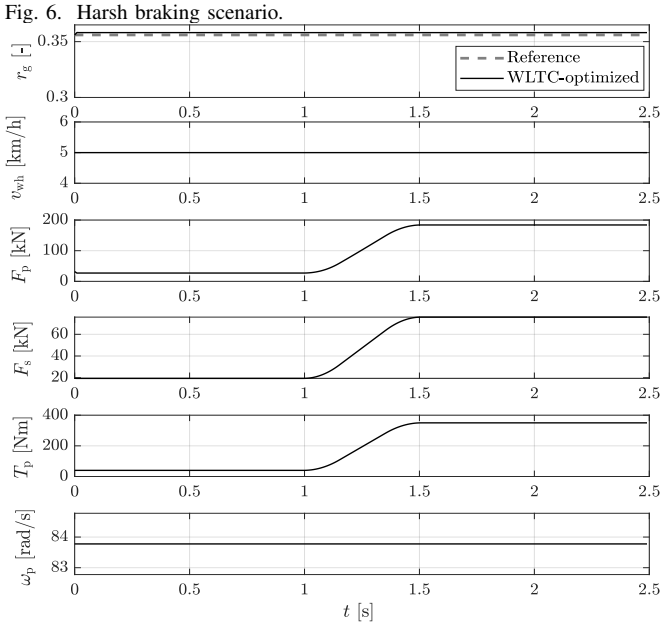

Fig. 8. Pressure gradient scenario.

driving scenario, the leakage losses can be reduced. However, doing this may result in different plant design parameters, as will be explained in more detail in the subsequent subsection.

Finally, since the controller of Case 2 is optimized for the WLTC, it allows for higher leakage losses during some of the alternative driving maneuvers. This is confirmed by the results obtained for Case 4, where we optimize just the controller for each of the individual driving scenarios, given the plant design parameters obtained from co-design on the WLTC, as shown in Fig. 12.

D. Influence of Driving Scenarios on Optimized Design

In the previous subsection, we have evaluated the WLTC-optimized CVT design on various driving scenarios outside of the driving cycle. Now, we further investigate the effects of driving profiles on the obtained optimization results. We select a more aggressive scenario (tip-in) and we perform co-design with this profile. During this driving maneuver, the CVT is expected to perform a ratio shift to a low ratio value within a short amount of time, accommodating a sharp increase in input torque and speed. Similarly, we validate the obtained plant and control design parameters on the driving scenarios not utilized during the co-design process. For the sake of brevity, we demonstrate the results obtained with $w_{\mathrm{P}} = 0.4$, which is the point that yields $J_{\mathrm{P}} \leq 1$, $J_{\mathrm{C}} \leq 1$. The comparison of the obtained design parameters $\{\mathbf{x}_{\mathrm{P}}, \mathbf{x}_{\mathrm{C}}\}$ in more detail is summarized in Table III.

Based on the results, it becomes evident that when a more

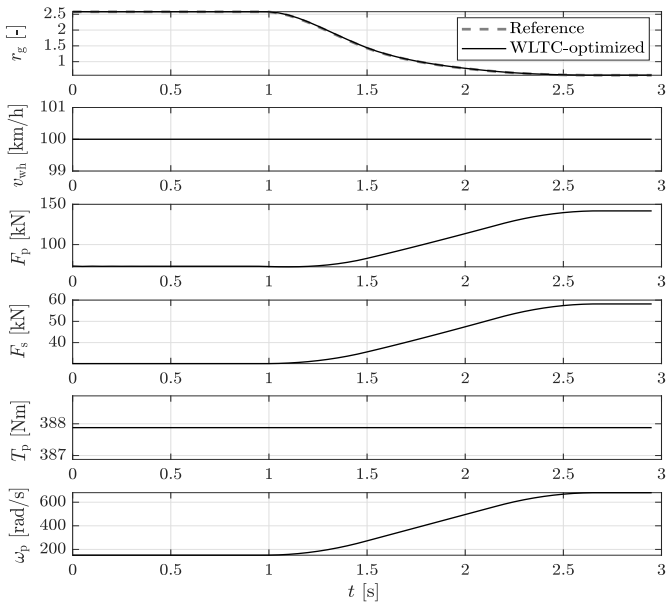

Fig. 9. Manual downshifting scenario.

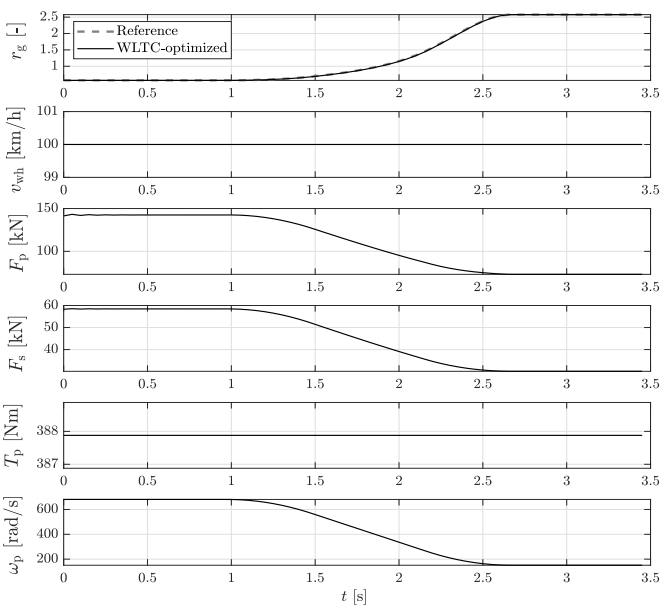

Fig. 10. Manual upshifting scenario.

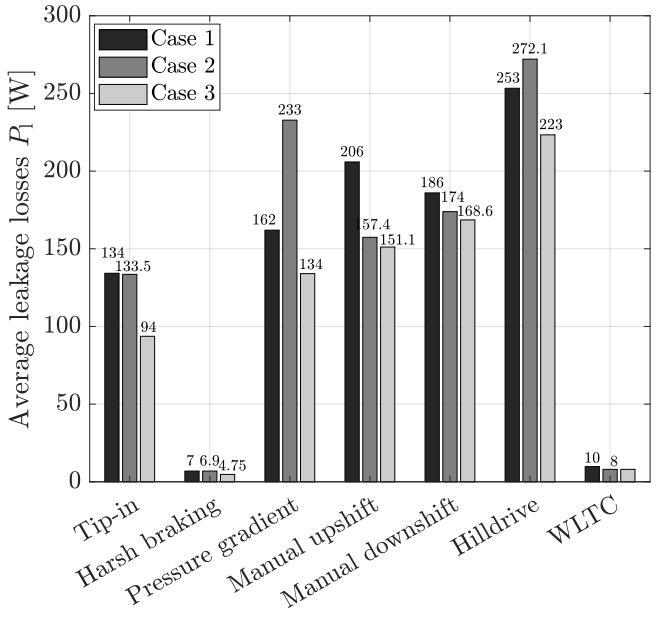

Fig. 11. Comparison of the average leakage loss for Case 1 (baseline plant parameters with controller optimized for each individual driving scenario); Case 2 (plant and control design parameters obtained from co-design on WLTC); Case 3 (plant and control design parameters obtained from co-design on each individual driving scenario).

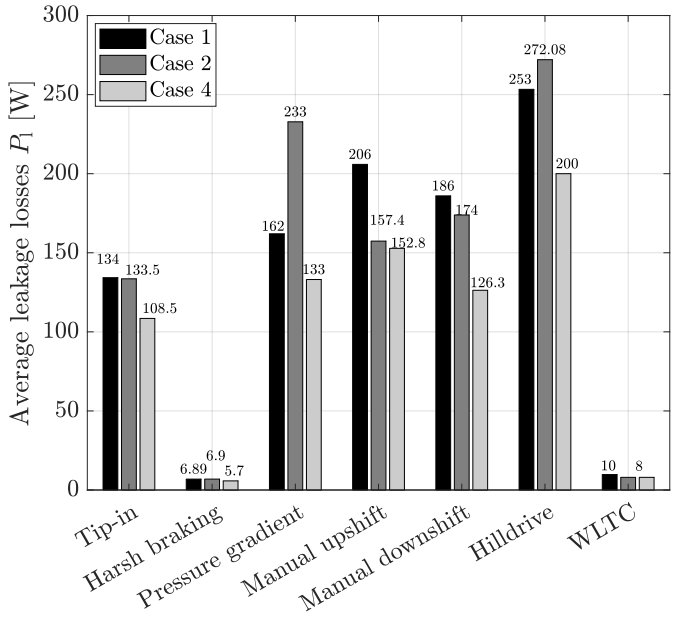

Fig. 12. Comparison of the average leakage loss for Case 1 (baseline plant parameters with controller optimized for each individual driving scenario); Case 2 (plant and control design parameters obtained from co-design on WLTC); Case 4 (plant design parameters obtained from co-design on WLTP, controller optimized for each individual driving scenario).

aggressive driving profile is used to perform plant and control design optimization, the resulting variator mass is higher than the results achieved for the WLTC scenario. Furthermore, it transpires that in terms of physical design, the optimized wedge angle β as well as the plant objective (variator mass) of the tip-in scenario is higher than that of the WLTC case. However, the estimated leakage energy for the tip-in case is slightly higher, as shown in Table. III. This demonstrates the influence of the selected driving profile on the obtained optimized design.

E. Pareto Frontier

The weighting factor w_{P} assigned during optimization plays a role in the importance of either the plant or control objective of the proposed design formulation. For various optimization weights, a Pareto Frontier for the computed optimized objective values J_{P} and J_{C} for different driving scenarios is displayed in Fig. 13. The results show that the variator mass

TABLE III
INFLUENCE OF DRIVING PROFILES

Parameters	WLTC-optimized	Tip-in-optimized	Unit
w_{P}	0.5	0.4	-
$M_{\mathrm{v}}^{\star}$	6.2	7.0	kg
$\beta^{\star}$	7	9.63	deg
$R_1^{\star}$	26.1	26.1	mm
$R_2^{\star}$	88.5	88.5	mm
$K_{\mathrm{p}}^{\star}$	214.6	31.8	1/s
$K_{\mathrm{i}}^{\star}$	0.4	2	1/s
E_{l} (WLTC)	1.4	1.5	kJ

TABLE IV
SIMULATION PARAMETERS

Parameters	Description	Value	Unit
$\underline{\beta}$	min. wedge angle	7	deg
$\underline{R}_1$	min. shaft radius	20	mm
$\underline{R}_2$	min. pulley radius	70	mm
$\underline{K}_{\mathrm{p}}$	min. controller gain	0.01	1/s
$\underline{K}_{\mathrm{i}}$	min. controller gain	0.01	1/s
$\underline{e}$	min. tracking error	-0.1	-
$\underline{r}_{\mathrm{g}}$	min. transmission ratio	0.356	-
$\overline{\beta}$	max. wedge angle	13	deg
$\overline{R}_1$	max. shaft radius	30	mm
$\overline{R}_2$	max. pulley radius	88.5	mm
$\overline{K}_{\mathrm{p}}$	max. controller gain	500	1/s
$\overline{K}_{\mathrm{i}}$	max. controller gain	500	1/s
$\overline{e}$	max. tracking error	0.1	-
$\overline{T}_{\mathrm{p}}$	max. input torque	220	Nm
$\overline{r}_{\mathrm{g}}$	max. transmission ratio	2.8	-
$C_{\mathrm{l,p}}$	pri. pulley leakage coefficient	3.63	$10^{-12}\,\mathrm{m}^5/(\mathrm{Ns})$
$C_{\mathrm{l,s}}$	sec. pulley leakage coefficient	1.04	$10^{-12}\,\mathrm{m}^5/(\mathrm{Ns})$
μ_{cvt}	CVT max. traction coefficient	0.09	-
ρ_{oil}	Oil density	850	$\mathrm{kg/cm}^3$
δ_{a}	min. pulley gap	3	mm
δ_{ou}	belt margin from pulley outer edge	4	mm
δ_{in}	belt margin from pulley inner edge	4	mm
$t_{\mathrm{ch,p}}$	oil chamber thickness	10	mm
f_{p}	piston radius constant	1.4	-

and leakage losses are two conflicting objectives. In other words, the more emphasis is placed on minimizing the plant design problem J_{P} (variator mass), the higher the resulting control cost J_{C}, and vice versa. The increase in leakage losses is mainly due to the reduced pulley outer radius (R_2), which results in a smaller hydraulic surface area. A smaller surface area yields higher clamping pressures that need to be supplied by hydraulic oil, and thereby results in greater leakage losses at the variator.

Furthermore, it can be noted that the Pareto Frontier of the proposed optimization problem is different for each of the driving scenarios investigated in this paper. Consequently, it was found that for the case of WLTC, the point which leads to both lower plant and control objectives when compared to those of the baseline ($J_{\mathrm{P}} \leq 1$, $J_{\mathrm{C}} \leq 1$) is obtained for $w_{\mathrm{P}} = 0.5$. However, for the case of tip-in, the corresponding point is $w_{\mathrm{P}} = 0.4$. This indicates that the driving profile in which a co-design of the CVT is performed, has a significant influence on the obtained optimization results.

V. CONCLUSIONS AND RECOMMENDATIONS

In this paper, a simultaneous integrated plant and control design (co-design) of a continuously variable transmission (CVT) has been presented. The aim of the new design is to obtain a more power dense CVT with a reduced variator mass, as well as minimizing the leakage losses while still meeting the required shifting performance during driving. We have proposed the design problem as a nonlinear multi-objective optimization formulation with a closed loop control structure based on feedback linearization.

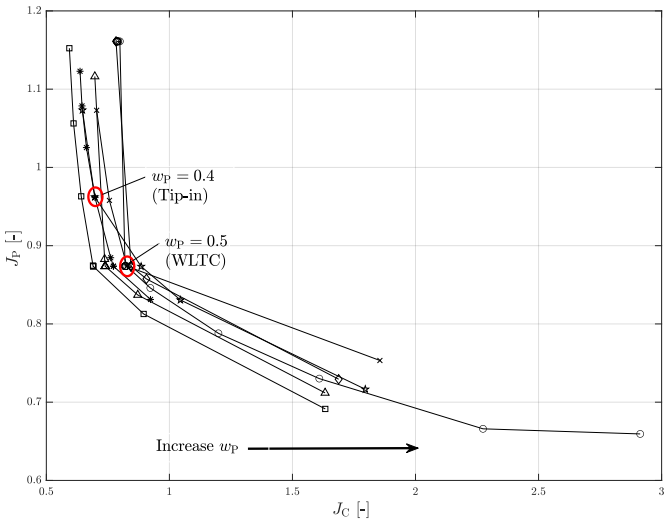

Fig. 13. Pareto frontier of the proposed design formulation for various optimization weights w_{P}.

We demonstrated that both the weight factor and driving cycle used during the optimization process have an influence on the results. Furthermore, our results show that reducing the pulley wedge angle yields several benefits, including a reduced transmission weight and a higher CVT power density. For the WLTC profile, up to 13% reduction in the CVT variator mass and 18% reduction in leakage loss are obtained with the proposed design framework. Moreover, due to the interdependence between the plant and the controller, changing the pulley wedge angle, the pulley sheave, and shaft diameters has to be done with caution, as such interventions can contribute to higher leakage loss at the variator level. This highlights the importance of performing design optimization of a complete system in an integrated fashion.

To this end, we aim to further extend this study to include other subsystems of the CVT, e.g., the actuation system. We are also keen to integrate the CVT design problem at the powertrain level, where the optimal sizing of the propulsion source (electric motor or engine) is also taken into account.

VI. ACKNOWLEDGEMENT

The authors would like to thank Dr. Ilse New for proof-reading this paper.

REFERENCES

[1] S. Barsali, C. Miulli, and A. Possenti, "A control strategy to minimize fuel consumption of series hybrid electric vehicles," *IEEE Transactions on Energy Conversion*, vol. 19, no. 1, pp. 187–195, 2004.

[2] S. Delprat, J. Lauber, T. M. Guerra, and J. Rimaux, "Control of a parallel hybrid powertrain: optimal control," *IEEE Transactions on Vehicular Technology*, vol. 53, no. 3, pp. 872–881, 2004.

[3] C.-C. Lin, H. Peng, J. W. Grizzle, and J.-M. Kang, "Power management strategy for a parallel hybrid electric truck," *IEEE Transactions on Control Systems Technology*, vol. 11, no. 6, pp. 839–849, 2003.

[4] V. H. Johnson, K. B. Wipke, and D. J. Rausen, "Hev control strategy for real time optimization of fuel economy and emissions," in *SAE World Congress*, 2000.

[5] J. Ritzmann, A. Christon, M. Salazar, and C. H. Onder, "Fuel-optimal power split and gear selection strategies for a hybrid electric vehicle," in *SAE Int. Conf. on Engines & Vehicles*, 2019.

[6] T. Hofman, M. Steinbuch, R. Van Druten, and A. Serrarens, "Rule-based energy management strategies for hybrid vehicles," *International Journal of Electric and Hybrid Vehicless*, vol. 1, no. 1, pp. 71–94, 2007.

[7] N. Robuschi, M. Salazar, P. Duhr, F. Braghin, and C. H. Onder, "Minimum-fuel engine on/off control for the energy management of hybrid electric vehicles via iterative linear programming," in *Symposium on Advances in Automotive Control*, 2019.

[8] C. Desai and S. Williamson, "Optimal design of a parallel hybrid electric vehicle using multi-objective genetic algorithms," in *IEEE Vehicle Power and Propulsion Conference*, 2009.

[9] O. Hegazy and J. van Mierlo, "Particle swarm optimization for optimal powertrain component sizing and design of fuel cell hybrid electric vehicle," in *Int. Conf. on Optimization of Electrical and Electronic Equipment*, 2010.

[10] L. Wang, E. Collins, and H. Li, "Optimal design and real-time control for energy management in electric vehicles," *IEEE Transactions on Vehicular Technology*, vol. 60, no. 4, pp. 1419 – 1429, 2011.

[11] E. Silvas, T. Hofman, N. Murgovski, P. Etman, and M. Steinbuch, "Review of optimization strategies for system-level design in hybrid electric vehicles," *IEEE Transactions on Vehicular Technology*, vol. 66, no. 1, pp. 57–70, 2016.

[12] T. Hofman and M. Salazar, "Transmission ratio design for electric vehicles via analytical modeling and optimization," in *IEEE Vehicle Power and Propulsion Conference*, 2020, in press.

[13] O. Borsboom, C. A. Fahdzyana, M. Salazar, and T. Hofman, "Time-optimal control strategies for electric race cars for different transmission technologies," in *IEEE Vehicle Power and Propulsion Conference*, 2020, in press.

[14] M. A. Kluger and D. M. Long, "An overview of current automatic, manual and continuously variable transmission efficiencies and their projected future improvements," in *SAE Technical Pape*, 1999.

[15] H. Fathy, J. Reyer, P. Papalambros, and A. Ulsoy, "On the coupling between the plant and controller optimization problems," in *American Control Conference*, 2001.

[16] H. Fathy, "Combined plant and control optimization: Theory, strategies and applications," Ph.D. dissertation, Univ. of Michigan, 2003.

[17] J. Allison, "Optimal partitioning and coordination decisions in decomposition-based design optimization," Ph.D. dissertation, Univ. of Michigan, 2008.

[18] J. Reyer, "Combined embodiment design and control optimization: Effects of cross-disciplinary coupling," Ph.D. dissertation, Univ. of Michigan, 2000.

[19] A. P. Deshmukh and J. T. Allison, "Multidisciplinary dynamic optimization of horizontal axis wind turbine design," *Structural and Multidisciplinary Optimization*, vol. 53, no. 1, pp. 15–27, 2016.

[20] J. T. Allison, "Plant-limited co-design of an energy-efficient counterbalanced robotic manipulator," *ASME Journal of Mechanical Design*, vol. 135, no. 10, p. 101003, 2013.

[21] S. F. Alyaqout, P. Y. Papalambros, and A. G. Ulsoy, "Combined design and robust control of a vehicle passive/active suspension," in *European Control Conference*, 2007.

[22] C. Shiau, N. Kaushal, C. Hendrickson, S. B. Peterson, J. Whitacre, and J. Michalek, "Optimal plug-in hybrid electric vehicle design and allocation for minimum life cycle cost, petroleum consumption, and greenhouse gas emissions," *ASME Journal of Mechanical Design*, vol. 132, no. 9, p. 091013, 2010.

[23] O. Sundström, L. Guzzella, and P. Soltic, "Optimal hybridization in two parallel hybrid electric vehicles using dynamic programming," in *IFAC World Congress*, 2008.

[24] M. Pourabdollah, E. Silvas, N. Murgovski, M. Steinbuch, and B. Egardt, "Optimal sizing of a series phev: Comparison between convex optimization and particle swarm optimization," in *IFAC Workshop on Engine and Powertrain Control, Simulation and Modeling*, 2015.

[25] Z. Ma, N. Murgovski, B. Egardt, and S. Cu, "Comprehensive analysis and optimal configurations of the evt powertrain," *IEEE Transactions on Vehicular Technology*, vol. 68, no. 10, pp. 9573 – 9587, 2019.

[26] E. Silvas, E. Bergshoeff, T. Hofman, and M. Steinbuch, "Comparison of bi-level optimization frameworks for sizing and control of a hybrid electric vehicle," in *IEEE Vehicle Power and Propulsion Conference*, 2014.

[27] H. K. Fathy, P. Y. Papalambros, A. G. Ulsoy, and D. Hrovat, "Nested plant/controller optimization with application to combined passive/active automotive suspensions," in *American Control Conference*, 2003.

[28] Z. Ma, S. Cui, and S. Li, "Applying dynamic programming to hev powertrain based on evt," in *Int. Conf. on Control, Automation and Information Sciences* , 2015.

[29] D. R. Herber and J. T. Allison, "Nested and simultaneous solution strategies for general combined plant and controller design problems," in *Int. Design Engineering Technical Conferences & Computers and Information in Engineering Conference*, 2017.

[30] J. Allison and Z. Han, "Co-design of an active suspension using simultaneous dynamic optimization," in *Int. Design Engineering Technical Conferences & Computers and Information in Engineering Conference*, 2011.

[31] A. Sari, C. Espanet, and D. Hissel, "Particle swarm optimization applied to the co-design of a fuel cell air circuit," *Journal of Power Sources*, vol. 179, no. 1, pp. 121–131, 2008.

[32] A. Deshmukh, D. Herber, and J. Allison, "Bridging the gap between open-loop and closed-loop control in co-design: A framework for complete optimal plant and control architecture design," in *American Control Conference*, 2015.

[33] T. W. G. L. Klaassen, "The empact cvt: dynamics and control of an electromechanically actuated cvt," Ph.D. dissertation, Technische Universiteit Eindhoven, 2007.

[34] A. Englisch, H. Faust, M. Homm, A. Teubert, and M. Vornehm, "Development of high performance cvt components," in *Int. Continuously Variable and Hybrid Transmission Congress*, 2004.

[35] A. Brandsma, J. van Lith, and E. Hendriks, "The cvt pushbelt reinvented for future compact and efficient powertrains," in *Int. Congress on Continuously Variable Power Transmission*, 1999.

[36] B. Bonsen, "Efficiency optimization of the push-belt cvt by variator slip control," Ph.D. dissertation, Technische Universiteit Eindhoven, 2006.

[37] C. Fahdzyana, S. van Raemdonck, and T. Hofman, "Joined plant and control design for continuous variable transmission systems," in *American Control Conference*, 2020.

[38] T. Ide, A. Udagawa, and R. Kataoka, "A dynamic response analysis of a vehicle with a metal v-belt cvt," in *Int. Symp. on Advanced Vehicle Control*, 1994.

[39] E. Shafai, M. Simons, and H. P. Neff, U.and Geering, "Model of a continuously variable transmission," in *Advances in Automotive Control*, 1995.

[40] G. Carbone, L. Mangialardi, B. Bonsen, C. Tursi, and P. A. Veenhuizen, "Cvt dynamics: Theory and experiments," *Mechanism and Machine Theory*, vol. 42, no. 4, pp. 409–428, 2007.

[41] S. van der Meulen, "High-performance control of continuously variable transmissions," Ph.D. dissertation, Technische Universiteit Eindhoven, 2010.

[42] B. Vroemen, "Component control for the zero inertia powertrain," Ph.D. dissertation, Technische Universiteit Eindhoven, 2001.

[43] A. Bieniek, M. Graba, and K. Praznowksi, "The influence of the pressure force control signal on selected parameters of the vehicle continuously variable transmission," in *Scientific Conference on Automotive Vehicles and Combustion Engines*, 2016.

[44] T. Kim, H. Kim, J. Yi, and H. Cho, "Ratio control of metal belt cvt," in *SAE World Congress*, 2000.

[45] M. Ye and Y. Liu, Y. G.and Cheng, "Modeling and ratio control of an electromechanical continuously variable transmission," *Int. Journal of Automotive Technology*, vol. 17, no. 2, pp. 225–235, 2016.

[46] H. K. Khalil, *Nonlinear Systems*, 3rd ed. Prentice Hall, 2002.

[47] J. Löfberg, "YALMIP : A toolbox for modeling and optimization in MATLAB," in *IEEE Int. Symp. on Computer Aided Control Systems Design*, 2004.

[48] A. Wächter and L. Biegler, "On the implementation of a primal-dual interior point filter line search algorithm for large-scale nonlinear programming," *Mathematical Programming*, vol. 106, no. 1, pp. 25–57, 2006.

[49] J. Currie and D. I. Wilson, "Opti: Lowering the barrier between open source optimizers and the industrial matlab user," in *Foundations of Computer Aided Process Operations / Chemical Process Control*, 2012.

Chyannie Amarillio Fahdzyana obtained the B.Sc. degree in Electrical Engineering from the University of Indonesia in 2015, and the M.Sc. degree in Automotive Technology from Eindhoven University of Technology, Eindhoven (TU/e), The Netherlands, in 2017. She is currently working towards a Ph.D. degree at the Control Technology Group of the same university. Her main research interests include optimal system design, optimization and optimal control.

Mauro Salazar is an Assistant Professor in the Control Systems Technology group at Eindhoven University of Technology (TU/e). He received the Ph.D. degree in Mechanical Engineering from ETH Zürich in 2019. Before joining TU/e he was a Postdoctoral Scholar in the Autonomous Systems Lab at Stanford University. Dr. Salazar's research is at the interface of control theory and optimization, and is aimed at the development of a comprehensive set of tools for the design, the deployment and the operation of sustainable mobility systems. Dr. Salazar received the Outstanding Bachelor Award and the Excellence Scholarship and Opportunity Award from ETH Zürich. Both his Master thesis and PhD thesis were recognized with the ETH Medal, and he was granted the Best Student Paper award at the 2018 Intelligent Transportation Systems Conference.

Theo Hofman was born in Utrecht, The Netherlands, in 1976. He received his M.Sc. (with honors) in 1999 and Ph.D.-degree in 2007 both in Mechanical Engineering from Eindhoven University of Technology, Eindhoven. From 1999 to 2003, he was a researcher and project manager with the R&D Department of Thales–Cryogenics B.V., Eindhoven, The Netherlands. From 2003 to 2007, he was a scientific researcher at Drivetrain Innovations B.V., Eindhoven. Since 2010, he is an Assistant Professor with the Control Systems Technology group. His research interests are system design optimization methods for complex dynamical engineering systems and discrete topology design using computational design synthesis.